Published in final edited form as:
Cell Metab. 2014 September 2; 20(3): 458–470. doi:10.1016/j.cmet.2014.06.015.

The ER-Associated Degradation Adaptor Protein Sel1L Regulates LPL Secretion and Lipid Metabolism

Haibo Sha[1], **Shengyi Sun**[2], **Adams Francisco**[3], **Nicole Ehrhardt**[4], **Zhen Xue**[1], **Lei Liu**[1], **Peter Lawrence**[1], **Frits Mattijssen**[5], **Robert Guber**[1], **Muhammad S. Panhwar**[6], **J. Thomas Brenna**[1], **Hang Shi**[7], **Bingzhong Xue**[7], **Sander Kersten**[1,5], **André Bensadoun**[1], **Miklós Péterfy**[4,8,10], **Qiaoming Long**[9,10], and **Ling Qi**[1,2,10,*]

[1]Division of Nutritional Sciences, Cornell University, Ithaca, NY 14853, USA [2]Graduate Program in Biochemistry, Molecular and Cell Biology, Cornell University, Ithaca, NY 14853, USA [3]Department of Animal Science, Cornell University, Ithaca, NY 14853, USA [4]Medical Genetics Research Institute, Cedars-Sinai Medical Center, Los Angeles, CA 90095, USA [5]Division of Human Nutrition, Wageningen University, 6703HD, Wageningen, The Netherlands [6]Weill Cornell Medical College in Qatar, Education City, PO Box 24144, Doha, Qatar [7]Department of Biology, Georgia State University, Atlanta, GA 30303, USA [8]Department of Medicine, University of California, Los Angeles, CA 90048, USA [9]Laboratory Animal Research Center, Medical College of Soochow University, Suzhou 215006, Jiangsu, China

SUMMARY

Sel1L is an essential adaptor protein for the E3 ligase Hrd1 in the endoplasmic reticulum-associated degradation (ERAD), a universal quality-control system in the cell; but its physiological role remains unclear. Here we show that mice with adipocyte-specific Sel1L deficiency are resistant to diet-induced obesity and exhibit postprandial hypertriglyceridemia. Further analyses reveal that Sel1L is indispensable for the secretion of lipoprotein lipase (LPL), independently of its role in Hrd1-mediated ERAD and ER homeostasis. Sel1L physically interacts and stabilizes the LPL maturation complex consisted of LPL and lipase-maturation factor 1 (LMF1). In the absence of Sel1L, LPL is retained in the ER and form protein aggregates, which are degraded primarily by autophagy. The Sel1L-mediated control of LPL secretion is also seen in

*CORRESPONDENCE:lq35@cornell.edu.
10co-senior authors

AUTHOR CONTRIBUTIONS L.Q. and H.S. designed the experiments with the input from A.B. and M.P.; H.S. performed and analyzed most of the experiments; H.S., S.S. and Z.X. generated AKO, IKO, and MKO mice, respectively; R.G. and M.S.P. measured adipocyte cell size and performed some protein interaction analysis; A.F. and Q.L. generated and provided Sel1L floxed mice; L.L., P.L., J.T.B. performed mass spec analysis of lipids; H.S. and B.X. provided the adiponectin-Cre mice on the B6 background; F.M., S.K. performed lipoprotein fractionation; A.B. involved in discussion, provided LPL antibody and analyzed LPL ELISA; N.E. and M.P. generated *Lmf1* mice, provided *Lmf1*$^{-/-}$ WAT and analyzed LPL activity; L.Q. and H.S. wrote the paper, R.G., S.K. and M.P. edited the paper, and everybody approved the manuscript.

The authors declare no competing financial interests.

other LPL-expressing cell types including cardiac myocytes and macrophages. Thus, our study reports a role of Sel1L in LPL secretion and systemic lipid metabolism.

Keywords

Adipocytes; diet-induced obesity; hypertriglyceridemia; ER; Sel1L-Hrd1 ERAD complex; LPL; autophagy

INTRODUCTION

Protein misfolding and aggregation in the endoplasmic reticulum (ER) contributes significantly to the etiology and pathogenesis of many devastating diseases, including type-1 diabetes, Creuzfeld-Jacob disease and cystic fibrosis (Chiti and Dobson, 2006). ER-associated degradation (ERAD) targets misfolded secretory and membrane proteins for proteasomal degradation (Olzmann et al., 2012), while autophagy may be responsible for the clearance of protein aggregates in the ER (Houck et al., 2012). Failure to degrade misfolded proteins in the ER leads to ER stress, activates unfolded protein response (UPR), and initiates global changes in transcription and translation (Hetz, 2012). Together, they represent key quality-control systems in the cell to maintain ER homeostasis and adjust ER capacity in response to environmental cues. Despite recent advances in the identification of many ERAD components (Olzmann et al., 2012), little is known about their physiological roles as to date studies of ERAD mouse models have been very limited.

Hrd3 or its mammalian homolog Sel-1 suppressor of lin-12-like protein (Sel1L) is an ER-resident transmembrane protein previously characterized as an adaptor protein for the E3 ligase hydroxymethylglutaryl reductase degradation protein 1 (Hrd1) (Gardner et al., 2000; Grant and Greenwald, 1996; Hampton et al., 1996; Sundaram and Greenwald, 1993). Within the ER, the Hrd3/Sel1L-Hrd1 complex targets a subset of misfolded or unfolded proteins for proteasomal degradation (Gardner et al., 2000; Mueller et al., 2008; Mueller et al., 2006). In mice, loss of Sel1L leads to embryonic lethality (Francisco et al., 2010), pointing to its importance in mammalian development. Using inducible mouse and cell models, we recently showed that Sel1L controls Hrd1 stability (similar to yeast homologs) and is indispensable for ER homeostasis and ERAD in adult mice (Sun et al., 2014). However, cell type-specific function of Sel1L and ERAD remains unknown.

LPL controls systemic lipid partitioning that is essential for energy homeostasis of the body. LPL is most abundantly expressed in adipose tissue, macrophages, heart and skeletal muscle, where it acts as a gatekeeper for the entry of fatty acids into tissues (Williams, 2008). LPL-mediated hydrolysis of dietary triglycerides packaged in chylomicrons is increased at adipose tissues during feeding (to increase lipid storage), but suppressed during fasting (Williams, 2008). Production of active LPL is tightly regulated at multiple stages (Dijk and Kersten, 2014; Doolittle and Peterfy, 2010; Wang and Eckel, 2009), one of which is in the ER. Various ER chaperones are required for the folding of nascent LPL polypeptides into properly folded dimeric state (Ben-Zeev et al., 1992; Ben-Zeev et al., 2002; Vannier and Ailhaud, 1989). Lipase-maturation factor 1 (LMF1), an ER-resident five-transmembrane protein, interacts with LPL and promotes the maturation of LPL dimers

before the exit from the ER (Peterfy, 2012; Peterfy et al., 2007). In the absence of LMF1, LPL forms aggregates, becomes transport-incompetent and retained in the ER (Peterfy et al., 2007). Defects in LPL maturation in the ER result in hypertriglyceridemia known as familial hyperchylomicronemia, which contribute to the development of heart diseases, metabolic syndrome and other diseases in humans (Doolittle and Peterfy, 2010). Despite decades of effort, the maturation and secretion processes of LPL in the ER remain poorly understood.

Interestingly, adipocyte-specific Sel1L deficient mice (AKO hereafter) are resistant to diet-induced obesity and develop postprandial hypertriglyceridemia. Further investigations reveal an unexpected role of Sel1L in regulating LPL secretion, independently of its canonical role in Hrd1 and ERAD, not only in adipocytes, but also in macrophages and myocytes. Thus, Sel1L forms distinct functional complexes with Hrd1 and LPL.

RESULTS

Generation of AKO Mice

In vivo, Sel1L protein was highly expressed in the pancreas, liver, white adipose tissue (WAT), and moderately in brown adipose tissue (BAT), predominantly as an endoglycosidase H (endoH)-sensitive protein (Figure S1A), pointing to its ER localization. During adipogenesis, both Sel1L and Hrd1 were highly induced (Figures S1B-C). Stable knockdown of Sel1L or Hrd1 in 3T3-L1 preadipocytes had no noticeable effect on adipogenesis (Figures S1D-E), suggesting that they are dispensable for adipocyte differentiation. Both Sel1L and Hrd1 are constitutively expressed in WAT (Figure S1F). Interestingly, Sel1L protein level was induced by 50% upon refeeding with high-fat diet (HFD) in a transcription-independent manner (Figures S1F-G). This was not seen when mice were refed with low-fat diet (LFD) (Figure S1H). Thus, these data imply a possible role of Sel1L in lipid metabolism in mature adipocytes.

We generated AKO mice by crossing the *Sel1L*$^{flox/flox}$ mice with the Cre transgenic animals under the control of adipocyte-specific adiponectin promoter (Figure S1I). AKO mice and control littermates *Sel1L*$^{flox/flox}$ (WT) were born at the expected Mendelian ratios (Figure S1J). For some studies, we also generated adipocyte-specific heterozygous mice (HET) using a different breeding scheme (Figure S1K). Reduction of Sel1L protein level was limited to WAT and BAT, and in the case of WAT, specifically in adipocytes not stromal vesicular cells (SVC) (Figures 1A-B and S1L).

Resistance to Diet-Induced Obesity of AKO Mice

AKO and WT littermates, both males and females, grew comparably on LFD for the first 20 weeks of age (Figure S2A). To study the role of Sel1L in obesity, we placed 6-week-old AKO and WT littermates on HFD. Strikingly, both male and female AKO mice were resistant to HFD-induced obesity (Figures 1C-D). Dual energy X-ray absorptiometry (DEXA) analyses revealed a great reduction in fat mass, but not the lean mass, in AKO mice compared to WT mice following chronic HFD feeding (Figure 1E). Indeed, following 16-week HFD, epididymal fat (EF) of AKO mice weighed 67% less than that of the WT littermates (Figures 1F-G). Tissue histology revealed smaller epididymal adipocytes of AKO

mice (Figures 1H-I). Intriguingly, the livers of AKO mice were enlarged and developed steatosis with elevated triglyceride (TG) contents (Figures 1J-L). Moreover, serum TG levels of AKO mice on HFD were significantly higher than that of WT littermates (Figure 1M).

These changes were associated with elevated serum insulin levels (Figure 1N) and accordingly, increased expression of a subset of *de novo* lipogenic genes in both the liver and WAT of AKO mice on HFD (Figures S2B-C). Despite body weight difference, fasting glucose as well as glucose and insulin tolerance was comparable between the two cohorts (Figures 1O-Q). Levels of AKT phosphorylation in the liver and muscle under either *ad libitum* or post-insulin challenge conditions were comparable between the two cohorts (Figure S2D-F). Moreover, food intake (Figure S2G), fecal energy recovery (Figures S2H-I) and physical activity (Figure S2J) were comparable between the two cohorts. Interestingly, while respiratory quotient (RQ) was similar, both oxygen (O_2) consumption and carbon dioxide (CO_2) production were higher in AKO mice on HFD than WT littermates (Figures S2K-M), suggesting increased metabolic rate in AKO mice. Providing further support, rectal temperature of AKO mice was higher than WT controls under fasting or cold conditions (Figures S2N-O). Thus, we conclude that AKO mice are resistant to diet-induced obesity with lipid partitioning defect and that increased metabolic rate and thermogenesis may contribute, at least in part, to the lean phenotype of AKO mice on HFD.

Postprandial Hypertriglyceridemia in AKO Mice

We next addressed whether adipose tissues of AKO mice are intrinsically defective in lipid absorption. To circumvent body weight differences in HFD mice, we measured serum TG levels in LFD-fed littermates with similar body weights under fasting and refeeding conditions. There was no difference in fasting plasma TG and glycerol levels (Figures 2A-B). However, plasma TG levels in AKO mice were significantly higher than WT mice upon refeeding with either LFD or HFD by 50% or 2-fold, respectively (Figures 2C-D). Oral gavage of olive oil also led to hypertriglyceridemia in AKO mice (Figure 2E). Fast protein liquid chromatography (FPLC) analysis of fasting and refeeding plasma indicated that plasma TG-rich lipoproteins were comparable between the two cohorts during fasting but significantly increased in AKO mice following refeeding (Figure 2F). Plasma high-density lipoprotein (HDL)-cholesterol remained unchanged regardless of the feeding status (Figure 2G). Thus, AKO mice on HFD exhibit postprandial hypertriglyceridemia.

ER Retention and Accumulation of LPL in the Absence of Sel1L

Given the known role of LPL in postprandial hypertriglyceridemia (Wang and Eckel, 2009), we examined the status of LPL. Following refeeding, AKO mice exhibited lower post-heparin plasma LPL activity and mass compared to those of WT mice (Figures 3A-B). The moderate change was expected given relatively small proportion of LPL in WAT in total LPL pool. While tissue *Lpl* mRNA levels were comparable (Figures 3C and S3A), total LPL protein level was 2-3 fold higher in WAT of AKO mice on either LFD or HFD (Figures 3D and S3B). The observation that LPL levels were lower in plasma but higher in WAT suggested a possible defect in LPL secretion. Indeed, LPL protein was retained intracellularly: LPL secretion by primary adipocytes isolated from AKO mice was only

10-20% of that of WT mice, despite a 9-fold higher intracellular LPL levels (Figures 3E and S3C). The secretory defect seemed to be LPL specific as secretion of adiponectin was normal in AKO adipocytes (Figure 3E), and as general secretion was not affected in AKO adipocytes (Figure S3D). Thus, our data show that Sel1L is indispensable for LPL secretion in adipocytes.

Serendipitously, we noticed that LPL from adipose tissue and primary adipocytes of AKO mice migrated faster than that from WT samples following prolonged running of the SDS-PAGE (Figure 3F). This finding prompted us to examine the glycosylation status of LPL. LPL is first synthesized, glycosylated and undergoes partial trimming of oligosaccharide chains in the ER, and then transported to the Golgi where it is subject to trimming of mannose residues and conversion of LPL oligosaccharides into complex types (Ben-Zeev et al., 2002; Liu et al., 1993). Mouse LPL has two potential N-linked glycosylation sites required for the formation of active homodimer in the ER. The high-mannose form of glycans found in the ER is endoglycosidase H (endoH) sensitive whereas the complex form of glycans found in the Golgi apparatus or cell surface is endoH resistant; a mixture of the two in the Golgi gives an intermediate phenotype (Vannier and Ailhaud, 1989). Strikingly, the majority (~83%) of LPL protein in AKO WAT was endoH-sensitive, two times higher than that in WT WAT (Figure 3G), suggesting that Sel1L deficiency may lead to the ER-retention of LPL. This conclusion was further confirmed biochemically using ER fractionation (Figure 3H).

To explore possible physiological significance of Sel1L, we assessed the LPL status in WAT and BAT during the fasting-feeding transition and cold exposure, respectively. Refeeding increased total LPL protein levels in WAT of both WT and AKO mice (Figures 3I and S3E), suggesting that AKO mice respond to feeding normally. However, refeeding doubled the proportions of the endoH-resistant form of LPL in WT WAT, but not in AKO WAT (Figures 3I and S3E). In BAT, cold exposure increased both total and endoH resistant form of LPL in WT mice, but not in AKO mice (Figures 3J and S3F).

To further determine whether the effect of Sel1L on LPL secretion is a general phenomenon, we examined the LPL behavior in other LPL-expressing cells, including macrophages and myocytes. Similar to the situation in AKO adipocytes, Sel1L-deficient bone marrow derived macrophages (BMDM) from myeloid-specific Sel1L deficient (MKO) mice exhibited increased total LPL protein levels, most of which were endoH sensitive (Figure 3K). Consistently, LPL secretion was reduced by 80% in MKO BMDM when compared to that of WT cells (Figure 3L). Moreover, using cardiac muscle from the inducible Sel1L knockout mice (IKO) we recently generated (Sun et al., 2014), we observed that LPL accumulated by 2-3-fold upon acute deletion of Sel1L, the majority of which was endoH sensitive (Figures 3M-N). Thus, our data establish that Sel1L is involved in LPL secretion.

Defective ERAD and Elevated UPR in WAT of AKO Mice

We next explored possible molecular mechanism underlying Sel1L-mediated regulation of LPL secretion. We first determined how Sel1L deficiency affects ERAD in adipocytes. In agreement with our earlier study (Sun et al., 2014), protein level of Hrd1 was greatly reduced while that of EDEM1 and both isoforms of OS9, bona fide substrates of the Sel1L-

Hrd1 ERAD complex (Sun et al., 2014), was dramatically elevated in WAT of AKO mice (Figure 4A). Turnover of OS9 protein was blocked in AKO adipocytes (Figure S4), pointing to a defective ERAD. Protein levels of other E3 ligases such as GP78 and RMA1 were not altered in WAT of AKO mice (Figure 4A and not shown). Thus, Sel1L is indispensable for the stability and function of Hrd1, and ERAD is compromised in the absence of Sel1L in adipocytes.

We next addressed whether ER homeostasis is disturbed in WAT of AKO mice. Western blot analysis revealed an increase of GRP78, ERO1L and eIF2α phosphorylation in WAT of AKO mice fed HFD compared to the WT cohorts (Figure 4B). Microarray analysis revealed that selective UPR/ERAD genes and pathways associated with ER homeostasis (e.g. ER protein processing, unfolded protein response, and chaperone activation by IRE1α) were highly upregulated (Figures 4C-D and S5A-B). Consistently, mild ER dilation was noted in white adipocytes of AKO mice fed HFD (Figure S5C). Quantitative PCR (qPCR) analysis further showed a mild induction of a subset of UPR genes, including *Grp78, Erdj4, P58ipk, Pdia6 and Ero1l* as well as *Xbp1* mRNA splicing in WAT of AKO mice (Figures 4E-F).

Although UPR has been linked to cell death and inflammation *in vitro* upon challenge with pharmacological drugs (Hotamisligil, 2010), we found no evidence of that in AKO mice as demonstrated by the protein levels of Caspase3 cleavage and ATF3, an inflammation-responsive gene involved in apoptosis (Hartman et al., 2004) (Figure 4G). In addition, expression of inflammatory genes and JNK phosphorylation in WAT and serum levels of inflammatory cytokines such as IL-6, and TNFα were not affected by Sel1L deficiency (Figures 4H and S5D-E). Thus, Sel1L deficiency in WAT is associated with ERAD defect and mild UPR, uncoupled from inflammation and cell death.

ER Stress-Independent Haploinsufficiency of Sel1L on LPL Secretion

To determine whether UPR accounts for reduced LPL secretion in Sel1L-deficient adipocytes, we addressed whether ER stress is sufficient to cause LPL accumulation. Primary adipocytes were treated with various ER stress inducers, including tunicamycin (Tm) and thapsigargin (Tg). Interestingly, neither drugs induced obvious LPL accumulation in adipocytes (Figure 4I). By contrast, when treated with brefeldin A (BFA) which blocks protein secretion, intracellular LPL level was elevated to a level similar to that of AKO adipocytes (Figure 4I).

We next addressed whether Sel1L affects LPL secretion in a dose-dependent manner using Sel1L HET mice. WAT of HET mice had reduced Sel1L and Hrd1 expression by 50% but no UPR activation as shown by protein levels of GRP78 and PDIA6 as well as eIF2α phosphorylation (Figure 4J). Interestingly, LPL behavior in WAT of HET mice exhibited an intermediate phenotype compared to those of WT and AKO mice, including total protein level, ER retention and secretion (Figures 4K-L). *In vivo*, HET mice exhibited intermediate postprandial hypertriglyceridemia (Figure 4M). Lastly, while knockdown of Sel1L by 60% in 3T3-L1 adipocytes didn't induce UPR (Figure S6A), it significantly impaired LPL secretion, but not adiponectin or adipsin (Figure S6B). Thus, these data demonstrate an ER stress-independent haploinsufficiency of Sel1L on LPL secretion.

Sel1L Regulates LPL Secretion Independently of Hrd1-Mediated ERAD

We next investigated whether LPL accumulation in AKO adipocytes is a direct result of ERAD dysfunction. To this end, we performed translational shut-off assays using a translation inhibitor cycloheximide (CHX) to assess the degradation rate of LPL in primary adipocytes. Despite reduced secretion, AKO adipocytes exhibited similar LPL decay as WT adipocytes (Figure 5A), suggesting that LPL degradation was not blocked by Sel1L deficiency. To determine whether LPL is degraded by proteasome/ERAD or lysosome/autophagy, we treated primary adipocytes with proteasome inhibitor MG132 or autophagy-specific inhibitors 3-methyladenine (3-MA) and chloroquine in addition to CHX. BFA was added to the culture medium to block LPL secretion. While MG132 had a minor effect on LPL stability (Figure 5B, lanes 12-14 and 26-28), treatment with 3-MA or chloroquine largely blocked LPL degradation in both WT and AKO adipocytes (Figure 5B, lanes 5-11 and 19-25) (quantitated in Figure 5C). Similar observations were obtained in 3T3-L1 adipocytes where chloroquine and 3-MA, but not MG132, attenuated LPL degradation (Figure 5D). Thus, in line with an earlier study (Ben-Zeev et al., 2002), proteasome-mediated ERAD does not play a major role in the clearance of LPL in adipocytes. Rather, our data show that autophagy is the primary mechanism for the clearance of LPL in adipocytes.

To further examine the role of the E3 ligase Hrd1 in LPL, we generated Hrd1-deficient adipocytes. Knockdown of Hrd1 by 90% in 3T3-L1 adipocytes failed to affect the secretion of LPL (Figures S6C-D). Taken together, our data demonstrate that ERAD and proteasome do not play a predominant role in LPL degradation, and that Sel1L-mediated regulation of LPL secretion is independent of Hrd1.

Sel1L Regulates the ER Exit of LPL and Prevents LPL Aggregation

During LPL maturation in the ER, there is a delicate balance between dimerization and aggregation (Ben-Zeev et al., 2002). To delineate how Sel1L deficiency affects LPL maturation, we performed sucrose-gradient sedimentation analysis to separate active LPL dimers from inactive high-molecular-weight (HMW) LPL-containing complexes in Triton X-100-soluble tissue lysates. While 84% of LPL was clustered in the dimer fractions of WT samples, only 46% of total LPL in AKO WAT was in the dimer fractions (Figure 6A). Conversely, over half of LPL in AKO WAT was in the HMW fractions vs. only 13% in WT WAT (Figure 6A). Next, we used a complementary approach to fractionate adipocyte lysates into soluble and insoluble form using a milder detergent NP40 (Sakakibara et al., 1997; Wang et al., 2011). Indeed, nearly 50% of LPL in AKO adipocytes at 4°C formed NP40-insoluble aggregates (NP40P), much higher than that in WT adipocytes (Figure 6B). Shifting culture temperature to 37°C increased LPL aggregation by over 50% in AKO adipocytes (Figure 6B), pointing to a dynamic formation of LPL aggregates in the absence of Sel1L. Protein aggregation is known to induce autophagy (Singh and Cuervo, 2012). Indeed, autophagic activity was increased in WAT of AKO mice as shown by elevated conversion of LC3-I to LC3-II (Figure 6C). Thus, Sel1L deficiency predisposes LPL to aggregate.

We next characterized LPL dimers in AKO adipocytes. We performed endoH analysis of the fractions from the sucrose gradient assay. Strikingly, 50% of LPL in the dimer fractions of the AKO sample was endoH sensitive vs. 9% in WT WAT (Figure 6D, lane 4 vs. 2), indicating that a large proportion of LPL dimers in AKO WAT were retained in the ER. Of note, for the HMW LPL, nearly all of them in AKO WAT were endoH sensitive vs. 43% in WT samples (Figure 6D, lanes 8 and 12 vs. 10).

We next compared LPL activity in WAT of LMF1- vs. Sel1L- deficient mice. As *Lmf1*-global knockout mice are embryonic lethal (M.P. et al, data not shown), we generated inducible *Lmf1*-deficient mice. LMF1 deficiency caused LPL accumulation in WAT, similar to that in AKO WAT (Figure 6E). Interestingly, while LMF1 deficiency abolished LPL activity, total LPL activity in WAT of AKO mice was higher than that of WT mice (Figure 6E). This data was in line with the amount of LPL dimers in AKO WAT (Figure 6A), suggesting that the dimers retained in the ER of AKO cells were active. Hence, LMF1 and Sel1L may affect different stages of LPL biogenesis: while LMF1 is required for LPL dimerization, Sel1L controls the ER exit of active LPL dimers.

Sel1L Forms a Complex with LPL-LMF1

To further dissect the molecular mechanism underlying the role of Sel1L on LPL, we determined whether Sel1L interacts with LPL. In HEK293T cells, exogenous and endogenous Sel1L protein interacted strongly with transfected LPL (Figures 7A and S7A). N-terminal domain (1-339 aa) of LPL that contains the lipolytic active site was sufficient to interact with Sel1L (Figure S7B). Sel1L also interacted with LMF1 in transfected HEK293T cells (Figure 7B). Interestingly, the interaction between LPL and LMF1 was dramatically augmented with the addition of Sel1L (Figure 7C, lanes 2 vs. 4 in panel c). On the other hand, LMF1 had no effect on the Sel1L-LPL interaction (Figure 7C, lanes 1 vs. 4 in panel e). Thus, these data suggest that Sel1L, LPL and LMF1 form a complex where Sel1L may help stabilize the complex.

We next asked whether Hrd1 is present in the Sel1L-LPL complex. Hrd1 interacted strongly with Sel1L (panel e) but not LPL (Figure 7D, panel d). Strikingly, addition of Hrd1 dramatically attenuated the Sel1L-LPL interaction (Figure 7D, lane 3 vs. 4 in panel f), suggesting that Hrd1 competes with LPL for Sel1L. Similarly, addition of Hrd1 also greatly reduced the interaction between Sel1L and LMF1 (Figure 7E, lane 3 vs. 4 in panel d), suggesting that Hrd1 competes with LMF1 for Sel1L.

DISCUSSION

Mammalian Sel1L is an essential component of the Hrd1 ERAD complex in vivo (Sun et al., 2014). Here our data demonstrate that Sel1L forms a functional complex with LPL-LMF1 on the ER membrane (Figure S7C). While the Sel1L-Hrd1 complex controls ERAD of misfolded proteins in the ER and thereby ER homeostasis, the Sel1L-LPL-LMF1 complex controls the ER exit and secretion of LPL dimers, thereby regulating systemic lipid partitioning (Figure 7F). Our data show that deficiency of Sel1L in adipocytes leads to not only ERAD deficiency and activation of UPR, but also intracellular retention of LPL and postprandial hypertriglyceridemia. The Sel1L-LPL-LMF1 complex helps stabilize nascent

LPL dimers and prevent aggregation, allowing the ER exit of LPL dimers. In the absence of Sel1L, LPL is trapped in the ER in the form of ERAD-resistant aggregates, which are degraded by autophagy.

Although LPL has been extensively studied in the last half century, how active LPL dimers are secreted from the ER remains a mystery. Investigation into hypertriglyceridemia of AKO mice has led us to the discovery of an unexpected function of Sel1L in LPL biology. Based on our data, we propose that Sel1L interacts with both LMF1 and LPL; upon the formation of active LPL dimers catalyzed by LMF1, Sel1L stabilizes LPL, prevents its aggregation and ensures the exit of transport-competent LPL from the ER (Figure 7F). In the absence of Sel1L, active LPL dimers are trapped and may dissociate into monomers, leading to aggregation (Figure 7F). Thus, Sel1L may act as a substrate-specific chaperone to stabilize LPL, similar to the situation for the E3 ligase Hrd1 (Gardner et al., 2000; Sun et al., 2014). In the future, more studies are required to further identify other Sel1L targets as well as protein components in the Sel1L-LPL complex.

Here we focused our attention on the role of Sel1L in LPL because of the novelty of this finding and because of its relevance to the hyperlipoproteinemia syndrome in humans. However, this is unlikely to be the sole role of Sel1L in adipose tissue as adipose-specific LPL-deficient mice on HFD exhibit a mild metabolic phenotype without changes in body and fat weights (Garcia-Arcos et al., 2013). Therefore, the lean phenotype of the AKO mice on HFD is likely due to other functions of Sel1L, such as UPR. Given that *Grp78*$^{+/-}$ mice exhibit a similar lean phenotype on HFD (Ye et al., 2010), we speculate that chronic UPR may lead to the resistance to diet-induced obesity in AKO mice. How alterations in ER homeostasis affect metabolic phenotype remains an interesting question. Our data showed that UPR in AKO mice is uncoupled from inflammation and cell death, thus excluding the possible involvement of the latter two in the resistance to diet-induced obesity. Future studies are required to elucidate the physiological role of Sel1L and the Sel1L-Hrd1 ERAD complex in WAT as well as in other tissues.

To date, little is known about the impact of the accumulation of misfolded proteins *in vivo* at the tissue and organismal levels. *In vitro*, when challenged with insurmountable ER stress induced by pharmacological drugs that causes the accumulation of misfolded proteins, cells undergo apoptosis through the activation of three branches of the UPR (Rutkowski and Kaufman, 2007). However, UPR associated with physiological conditions is likely to be mild. Our data show that the UPR induced by Sel1L and Hrd1 deficiency in adipocytes is well tolerated by the cell as mice appear largely normal at the first several months of life on LFD as well as the beginning several weeks of HFD feeding. Providing further support, inflammation and apoptosis are uncoupled from the UPR in WAT of AKO mice. The moderate UPR in AKO WAT may occur through three adaptive mechanisms. First, other components of E3 ERAD components (Smith et al., 2011) may compensate the Sel1L-Hrd1 defects. Indeed, a recent study showed the compensatory functions between the Hrd1 and Gp78 E3 ligases (Bernasconi et al., 2010). Second, elevated expression of ER chaperones and foldases in WAT of AKO mice is likely to increase folding capacity and reset homeostasis in the ER. Lastly, activation of PERK pathway in WAT and AKO mice may reduce the protein load into the ER. Thus, cellular adaption to the Sel1L-Hrd1 ERAD

deficiency in adipocytes may lead to a low-grade chronic UPR, uncoupled from apoptosis and inflammation. This conclusion may provide important insights into (patho)-physiological UPR.

Cell-type specific ERAD function remains largely unknown. Our data showed that adipocyte-specific Sel1L-deficient mice are resistant to diet-induced obesity and exhibit postprandial hypertriglyceridemia. As Sel1L deficiency also causes downregulation of Hrd1, our AKO mice indeed represent a Sel1L-Hrd1 double null mouse model. A recent study using liver-specific Hrd1 null mice showed that Hrd1 interacts and degrades Nrf2 to compromise antioxidant response in liver cirrhosis (Wu et al., 2014). Moreover, liver-specific gp78 null mice results in Insig-1/2 accumulation, thereby downregulating SREBP-mediated lipogenesis (Liu et al., 2012). The nature of the Sel1L-Hrd1 ERAD substrates requires further investigation.

Proteasome-mediated ERAD is the best characterized protein degradation pathways for misfolded proteins in the ER. One of the outstanding questions in the ERAD field is the substrate recognition by various ERAD complexes. In a recent study, we showed that OS9 and EDEM1, two chaperone proteins in the ER, accumulate in Sel1L-deficient pancreas (Sun et al., 2014). Similarly, OS9 and EDEM1 are highly upregulated in AKO WAT without transcriptional upregulation, indicative of an ERAD deficiency in AKO cells and pointing to OS9 and EDEM1 as Hrd1 substrates. By contrast, while LPL accumulates in the ER of Sel1L-deficient cells, it is not a result of ERAD deficiency and LPL is not a Sel1L-Hrd1 ERAD substrate. Rather, LPL is constitutively degraded by autophagy regardless of Sel1L status. LPL aggregation in Sel1L-deficient cells is due to the blockade of LPL secretion, rather than ERAD deficiency. This conclusion was further supported by our observation pointing to Sel1L haploinsufficiency on LPL secretion but not on UPR. Finally, using an overexpression system in HEK293T cells, our data show that Sel1L physically interacts with LPL and LMF1 and promotes the interaction between LPL and LMF1. While more studies are required to examine the formation of endogenous protein complex, these data provide strong evidence that Sel1L directly affects LPL secretion in the ER in an Hrd1/ERAD-independent manner.

Our data show that degradation of ER-retained LPL aggregates requires autophagy, in line with an earlier study (Ben-Zeev et al., 2002). This situation resembles what has been reported for the degradation of other ER-resident proteins such as apolipoprotein B100 and B48 (Ohsaki et al., 2006; Qiu et al., 2011), and abnormal ER proteins such as the α1 antitrypsin Z mutant (Hidvegi et al., 2010; Teckman and Perlmutter, 2000), gonadotropin-releasing hormone receptor mutants (Houck et al., 2014), and dysferlin (Fujita et al., 2007). A recent study suggested that downregulation of ERAD activity may promote the clearance of misfolded proteins in the ER via autophagy (Houck et al., 2014). Thus, autophagy may act to complement the function of the ERAD pathways to clear misfolded proteins or aggregates from the ER. However, how autophagy mediates the degradation of LPL aggregates remains unclear.

Increasing evidence suggests that persistent postprandial hypertriglyceridemia contributes to the development of atherosclerosis and coronary artery disease (Chan et al., 2013). Thus, our

findings may have therapeutic implications. Recent discovery of LMF1, GPIHBP1 and ANGPTL4 have provided key insights into LPL biology, where they play key roles at different stages of LPL maturation and function (Dijk and Kersten, 2014; Doolittle and Peterfy, 2010; Wang and Eckel, 2009). In this study, we have identified Sel1L as a modulator of LPL secretion from the ER. The LMF1-LPL-Sel1L interaction or Sel1L stability may be targeted therapeutically by small molecules to enhance the folding and secretion efficacy of LPL, hence reducing hyperlipidemia associated with metabolic syndrome.

EXPERIMENTAL PROCEDURES

Mice

Sel1L$^{flox/flox}$ mice has been recently described (Sun et al., 2014) and crossed with adiponectin promoter driven Cre mice (Eguchi et al., 2011) (gift from Dr. Evan Rosen), which have been backcrossed to the C57BL/6J background for more than 5 generations. Figures S1J-K show different breeding schemes to generate adipocyte-specific *Sel1L*$^{-/-}$ (AKO) and *Sel1L*$^{+/-}$ (HET) mice. Additionally, the *Sel1L*$^{flox/flox}$ animals were crossed with Lysozyme 2 promoter driven Cre mice on the B6 background (JAX 004781) to generate MKO mice. Inducible Sel1L-deficient mice (IKO) were generated and injected with tamoxifen as we recently described (Sun et al., 2014). All animal procedures associated with *Sel1L*-null mice have been approved by the Institutional Animal Care and Use Committee (IACUC) at Cornell University (#2007-0051). To generate mice with LMF1-deficient adipose tissue, mice carrying a floxed allele of *Lmf1* were crossed with tamoxifen-inducible Cre-transgenic mice (UBC-CreER, JAX #7001). LMF1 deficiency was induced by tamoxifen injections at 6 weeks of age. Studies with *Lmf1*-null mice were approved by the IACUC at the Cedars-Sinai Medical Center. Cohoused age- and gender-matched littermates were used in all *in vivo* experiments.

Metabolic Phenotyping

Blood glucose levels, glucose tolerance test (GTT, 1g glucose/KG body weight) and insulin tolerance test (ITT, 2U insulin/KG body weight) were performed as previously described (Sha et al., 2014). EF and livers were harvested, weighed and fixed for histology or snap-frozen for Western blot and qPCR. Fat and lean masses were measured using DEXA (PIXImus, GE Medical Systems Lunar) per manufacture's instruction. Blood was collected from jugular vein. Serum insulin levels were measured using the ELISA kit (Millipore) per supplier's protocol. TG levels in the plasma or serum were measured using Sigma GPO-Trinder kit (#TR0100, Sigma-Aldrich) per manufacture's instruction. To measure hepatic TG content, the liver was homogenized in 10 μl buffer (10 mM Tris-Cl, 2 mM EDTA, 0.25 M sucrose, pH 7.5) per mg of liver using Polytron (PRO Scientific). In a 96-well plate, 3 μl of homogenate was used for TG measurement. Lipoprotein profiling using FPLC was performed as previously described (Lichtenstein et al., 2007).

Plasma/Tissue LPL Mass and Activity

19-week-old female mice on LFD were fasted for 18 h followed by refeeding with HFD for 2 h. Mice were injected i.v. with 60 units (per mouse) of heparin sodium (VWR) in 0.9%

NaCl solution and blood was obtained from the retro-orbital plexus 10 min later. LPL levels in the post-heparin plasma were determined using ELISA as previously described (Weinstein et al., 2008). LPL activity was determined using a lecithin-stabilized radiolabeled triolein (glycerol tri[9,10(n)-^{3}H]oleate) substrate and normalized by total protein as described (Briquet-Laugier et al., 1999). WAT were collected from 16w-old WT and AKO female mice refed HFD for 3.5h following a 18h fast, as well as *Lmf1*$^{-/-}$ and their WT littermates fasted for 4h. WAT was homogenized at 100 mg/ml in a buffer containing 10 mM Tris-HCl, pH 7.5, 0.2% Na deoxycholate and 10 U/ml heparin, and protein concentration was assayed using the bicinchoninic acid (BCA) assay (Pierce).

LPL Secretion

Isolated primary adipocytes from WAT were plated at 30% (v/v) confluency in 6-well plates in KRBH buffer containing 1-2 μg/μl insulin (Sigma) and with or without 10 U/ml heparin. After culture for 4-6 h, medium was harvested and concentrated using Microsep 10K (PALL) and primary adipocytes were collected for cell lysates. Medium and cell lysates were subjected to Western blot analysis. Freshly differentiated BMDM from WT and MKO mice were prepared as previously described (Sun et al., 2012) and at day 6 were washed by PBS and incubated in DMEM medium supplemented with 2 mM intralipid and 10 U/ml heparin in the absence of serum for 3h. LPL levels in the cells and medium were determined as above.

Drug Treatment in Primary Adipocytes

Isolated primary adipocytes from WAT were plated at 30% (v/v) confluency in 6-well plates in KRBH buffer containing 1 μg/μl insulin and treated with various drugs including 5 μg/ml tunicamycin or 300 nM thapsigargin to induce ER stress, 1 μg/ml BFA to block protein secretion, 50 μg/ml CHX to block protein translation, 5 mM 3-MA or 200 μM chloroquine to inhibit autophagy, and 25 μM MG132 to inhibit proteasomal degradation. At the end of treatment, adipocytes and/or culture medium were collected for Western blots. For the translational shut-off assay (Figure 5B), primary adipocytes were maintained in KRBH buffer containing 1 μg/μl insulin and 1 μg/ml BFA for a total of 6 h, during which various combinations of drugs were added at 0, 2, 4 h. Cells were collected at the same time at the 6 h time point.

Statistical Analysis

Band density was quantitated using the Image Lab software on the ChemiDOC XRS^{+} system (Bio-Rad) or ImageJ (NIH). Experimental results are expressed as mean ± SEM. Comparisons between groups were made by unpaired two-tailed Student's *t* test, where $p < 0.05$ was considered as statistically significant. Gene Expression Omnibus (GEO) accession number for the microarray is GSE56918.

Supplementary Material

Refer to Web version on PubMed Central for supplementary material.

Acknowledgments

We thank Drs. Yihong Ye and Xuemei Han for reagents and technical assistance, and other members of the Qi Lab for assistance and discussion. This study was supported by Netherlands Organization for Health Research and Development ZonMW 40-00812-98-08030 (S.K.), NIH P01HL090553 (A.B.), R01HL-028481 (M.P.), Chinese National Science Foundation grant 31371391 (Q.L), NIH R01DK082582, American Diabetes Association (ADA) 07-08-JF-47 and 1-12-CD-04 (L.Q.). H.S. was a recipient of Genomics Scholarship from the Center for Vertebrate Genomics at Cornell University. S.S. is an International Student Research Fellow of the Howard Hughes Medical Institute (59107338). L.Q. is the recipient of the Junior Faculty and Career Development Awards from ADA.

REFERENCES

Ben-Zeev O, Doolittle MH, Davis RC, Elovson J, Schotz MC. Maturation of lipoprotein lipase. Expression of full catalytic activity requires glucose trimming but not translocation to the cis-Golgi compartment. J Biol Chem. 1992; 267:6219–6227. [PubMed: 1556130]

Ben-Zeev O, Mao HZ, Doolittle MH. Maturation of lipoprotein lipase in the endoplasmic reticulum. Concurrent formation of functional dimers and inactive aggregates. J Biol Chem. 2002; 277:10727–10738. [PubMed: 11796709]

Bernasconi R, Galli C, Calanca V, Nakajima T, Molinari M. Stringent requirement for HRD1, SEL1L, and OS-9/XTP3-B for disposal of ERAD-LS substrates. J Cell Biol. 2010; 188:223–235. [PubMed: 20100910]

Briquet-Laugier V, Ben-Zeev O, Doolittle MH. Determining lipoprotein lipase and hepatic lipase activity using radiolabeled substrates. Methods Mol Biol. 1999; 109:81–94. [PubMed: 9918014]

Chan DC, Pang J, Romic G, Watts GF. Postprandial hypertriglyceridemia and cardiovascular disease: current and future therapies. Current atherosclerosis reports. 2013; 15:309. [PubMed: 23345190]

Chiti F, Dobson CM. Protein misfolding, functional amyloid, and human disease. Annu Rev Biochem. 2006; 75:333–366. [PubMed: 16756495]

Dijk W, Kersten S. Regulation of lipoprotein lipase by Angptl4. Trends Endocrinol Metab. 2014; 25:146–155. [PubMed: 24397894]

Doolittle MH, Peterfy M. Mechanisms of lipase maturation. Clinical lipidology. 2010; 5:71–85. [PubMed: 20543905]

Eguchi J, Wang X, Yu S, Kershaw EE, Chiu PC, Dushay J, Estall JL, Klein U, Maratos-Flier E, Rosen ED. Transcriptional control of adipose lipid handling by IRF4. Cell Metab. 2011; 13:249–259. [PubMed: 21356515]

Francisco AB, Singh R, Li S, Vani AK, Yang L, Munroe RJ, Diaferia G, Cardano M, Biunno I, Qi L, Schimenti JC, Long Q. Deficiency of suppressor enhancer lin12 1 like (SEL1L) in mice leads to systemic endoplasmic reticulum stress and embryonic lethality. J Biol Chem. 2010; 285:13694–13703. [PubMed: 20197277]

Fujita E, Kouroku Y, Isoai A, Kumagai H, Misutani A, Matsuda C, Hayashi YK, Momoi T. Two endoplasmic reticulum-associated degradation (ERAD) systems for the novel variant of the mutant dysferlin: ubiquitin/proteasome ERAD(I) and autophagy/lysosome ERAD(II). Hum Mol Genet. 2007; 16:618–629. [PubMed: 17331981]

Garcia-Arcos I, Hiyama Y, Drosatos K, Bharadwaj KG, Hu Y, Son NH, O'Byrne SM, Chang CL, Deckelbaum RJ, Takahashi M, Westerterp M, Obunike JC, Jiang H, Yagyu H, Blaner WS, Goldberg IJ. Adipose-specific Lipoprotein Lipase Deficiency More Profoundly Affects Brown than White Fat Biology. J Biol Chem. 2013; 288:14046–14058. [PubMed: 23542081]

Gardner RG, Swarbrick GM, Bays NW, Cronin SR, Wilhovsky S, Seelig L, Kim C, Hampton RY. Endoplasmic reticulum degradation requires lumen to cytosol signaling. Transmembrane control of Hrd1p by Hrd3p. J Cell Biol. 2000; 151:69–82. [PubMed: 11018054]

Grant B, Greenwald I. The Caenorhabditis elegans sel-1 gene, a negative regulator of lin-12 and glp-1, encodes a predicted extracellular protein. Genetics. 1996; 143:237–247. [PubMed: 8722778]

Hampton RY, Gardner RG, Rine J. Role of 26S proteasome and HRD genes in the degradation of 3-hydroxy-3-methylglutaryl-CoA reductase, an integral endoplasmic reticulum membrane protein. Mol Biol Cell. 1996; 7:2029–2044. [PubMed: 8970163]

Hartman MG, Lu D, Kim ML, Kociba GJ, Shukri T, Buteau J, Wang X, Frankel WL, Guttridge D, Prentki M, Grey ST, Ron D, Hai T. Role for activating transcription factor 3 in stress-induced beta-cell apoptosis. Mol Cell Biol. 2004; 24:5721–5732. [PubMed: 15199129]

Hetz C. The unfolded protein response: controlling cell fate decisions under ER stress and beyond. Nat Rev Mol Cell Biol. 2012; 13:89–102. [PubMed: 22251901]

Hidvegi T, Ewing M, Hale P, Dippold C, Beckett C, Kemp C, Maurice N, Mukherjee A, Goldbach C, Watkins S, Michalopoulos G, Perlmutter DH. An autophagy-enhancing drug promotes degradation of mutant alpha1-antitrypsin Z and reduces hepatic fibrosis. Science. 2010; 329:229–232. [PubMed: 20522742]

Hotamisligil G. Endoplasmic reticulum stress and the inflammatory basis of metabolic disease. Cell. 2010; 140:900–917. [PubMed: 20303879]

Houck SA, Ren HY, Madden VJ, Bonner JN, Conlin MP, Janovick JA, Conn PM, Cyr DM. Quality Control Autophagy Degrades Soluble ERAD-Resistant Conformers of the Misfolded Membrane Protein GnRHR. Mol Cell. 2014; 54:166–179. [PubMed: 24685158]

Houck SA, Singh S, Cyr DM. Cellular responses to misfolded proteins and protein aggregates. Methods Mol Biol. 2012; 832:455–461. [PubMed: 22350905]

Lichtenstein L, Berbee JF, van Dijk SJ, van Dijk KW, Bensadoun A, Kema IP, Voshol PJ, Muller M, Rensen PC, Kersten S. Angptl4 upregulates cholesterol synthesis in liver via inhibition of LPL- and HL-dependent hepatic cholesterol uptake. Arterioscler Thromb Vasc Biol. 2007; 27:2420–2427. [PubMed: 17761937]

Liu G, Bengtsson-Olivecrona G, Olivecrona T. Assembly of lipoprotein lipase in perfused guinea-pig hearts. Biochem J. 1993; 292(Pt 1):277–282. [PubMed: 8503856]

Liu TF, Tang JJ, Li PS, Shen Y, Li JG, Miao HH, Li BL, Song BL. Ablation of gp78 in liver improves hyperlipidemia and insulin resistance by inhibiting SREBP to decrease lipid biosynthesis. Cell Metab. 2012; 16:213–225. [PubMed: 22863805]

Mueller B, Klemm EJ, Spooner E, Claessen JH, Ploegh HL. SEL1L nucleates a protein complex required for dislocation of misfolded glycoproteins. Proc Natl Acad Sci USA. 2008; 105:12325–12330. [PubMed: 18711132]

Mueller B, Lilley BN, Ploegh HL. SEL1L, the homologue of yeast Hrd3p, is involved in protein dislocation from the mammalian ER. J Cell Biol. 2006; 175:261–270. [PubMed: 17043138]

Ohsaki Y, Cheng J, Fujita A, Tokumoto T, Fujimoto T. Cytoplasmic lipid droplets are sites of convergence of proteasomal and autophagic degradation of apolipoprotein B. Mol Biol Cell. 2006; 17:2674–2683. [PubMed: 16597703]

Olzmann JA, Kopito RR, Christianson JC. The Mammalian Endoplasmic Reticulum-Associated Degradation System. Cold Spring Harbor perspectives in biology. 2012:5.

Peterfy M. Lipase maturation factor 1: A lipase chaperone involved in lipid metabolism. Biochim Biophys Acta. 2012; 1821:790–794. [PubMed: 22063272]

Peterfy M, Ben-Zeev O, Mao HZ, Weissglas-Volkov D, Aouizerat BE, Pullinger CR, Frost PH, Kane JP, Malloy MJ, Reue K, Pajukanta P, Doolittle MH. Mutations in LMF1 cause combined lipase deficiency and severe hypertriglyceridemia. Nat Genet. 2007; 39:1483–1487. [PubMed: 17994020]

Qiu W, Zhang J, Dekker MJ, Wang H, Huang J, Brumell JH, Adeli K. Hepatic autophagy mediates endoplasmic reticulum stress-induced degradation of misfolded apolipoprotein B. Hepatology. 2011; 53:1515–1525. [PubMed: 21360721]

Rutkowski DT, Kaufman RJ. That which does not kill me makes me stronger: adapting to chronic ER stress. Trends Biochem Sci. 2007; 32:469–476. [PubMed: 17920280]

Sakakibara A, Furuse M, Saitou M, Ando-Akatsuka Y, Tsukita S. Possible involvement of phosphorylation of occludin in tight junction formation. J Cell Biol. 1997; 137:1393–1401. [PubMed: 9182670]

Sha H, Yang L, Liu M, Xia S, Liu Y, Liu F, Kersten S, Qi L. Adipocyte spliced form of x-box-binding protein 1 promotes adiponectin multimerization and systemic glucose homeostasis. Diabetes. 2014; 63:867–879. [PubMed: 24241534]

Singh R, Cuervo AM. Lipophagy: connecting autophagy and lipid metabolism. Int J Cell Biol. 2012; 2012:282041. [PubMed: 22536247]

Smith MH, Ploegh HL, Weissman JS. Road to ruin: targeting proteins for degradation in the endoplasmic reticulum. Science. 2011; 334:1086–1090. [PubMed: 22116878]

Sun S, Shi G, Han X, Francisco AB, Ji Y, Mendonca N, Liu X, Locasale JW, Simpson KW, Duhamel GE, Kersten S, Yates JR 3rd, Long Q, Qi L. Sel1L is indispensable for mammalian endoplasmic reticulum-associated degradation, endoplasmic reticulum homeostasis, and survival. Proc Natl Acad Sci U S A. 2014; 111:E582–591. [PubMed: 24453213]

Sun S, Xia S, Ji Y, Kersten S, Qi L. The ATP-P2X7 Signaling Axis Is Dispensable for Obesity-Associated Inflammasome Activation in Adipose Tissue. Diabetes. 2012; 61:1471–1478. [PubMed: 22415881]

Sundaram M, Greenwald I. Suppressors of a lin-12 hypomorph define genes that interact with both lin-12 and glp-1 in Caenorhabditis elegans. Genetics. 1993; 135:765–783. [PubMed: 8293978]

Teckman JH, Perlmutter DH. Retention of mutant alpha(1)-antitrypsin Z in endoplasmic reticulum is associated with an autophagic response. Am J Physiol Gastrointest Liver Physiol. 2000; 279:G961–974. [PubMed: 11052993]

Vannier C, Ailhaud G. Biosynthesis of lipoprotein lipase in cultured mouse adipocytes. II. Processing, subunit assembly, and intracellular transport. J Biol Chem. 1989; 264:13206–13216. [PubMed: 2753912]

Wang H, Eckel RH. Lipoprotein lipase: from gene to obesity. Am J Physiol Endocrinol Metab. 2009; 297:E271–288. [PubMed: 19318514]

Wang Q, Liu Y, Soetandyo N, Baek K, Hegde R, Ye Y. A ubiquitin ligase-associated chaperone holdase maintains polypeptides in soluble states for proteasome degradation. Mol Cell. 2011; 42:758–770. [PubMed: 21636303]

Weinstein MM, Yin L, Beigneux AP, Davies BS, Gin P, Estrada K, Melford K, Bishop JR, Esko JD, Dallinga-Thie GM, Fong LG, Bensadoun A, Young SG. Abnormal patterns of lipoprotein lipase release into the plasma in GPIHBP1-deficient mice. J Biol Chem. 2008; 283:34511–34518. [PubMed: 18845532]

Williams KJ. Molecular processes that handle -- and mishandle -- dietary lipids. J Clin Invest. 2008; 118:3247–3259. [PubMed: 18830418]

Wu T, Zhao F, Gao B, Tan C, Yagishita N, Nakajima T, Wong PK, Chapman E, Fang D, Zhang DD. Hrd1 suppresses Nrf2-mediated cellular protection during liver cirrhosis. Genes Dev. 2014; 28:708–722. [PubMed: 24636985]

Ye R, Jung DY, Jun JY, Li J, Luo S, Ko HJ, Kim JK, Lee AS. Grp78 Heterozygosity Promotes Adaptive Unfolded Protein Response and Attenuates Diet-Induced Obesity and Insulin Resistance. Diabetes. 2010; 59:6–16. [PubMed: 19808896]

HIGHLIGHTS

- Adipocyte-specific Sel1L-deficient mice (AKO) are resistant to diet-induced obesity
- AKO mice on HFD exhibit postprandial hypertriglyceridemia
- Sel1L stabilizes and prevents LPL dimers from aggregation in the ER
- Sel1L forms a complex with LPL and LMF1 to regulate the ER exit of LPL

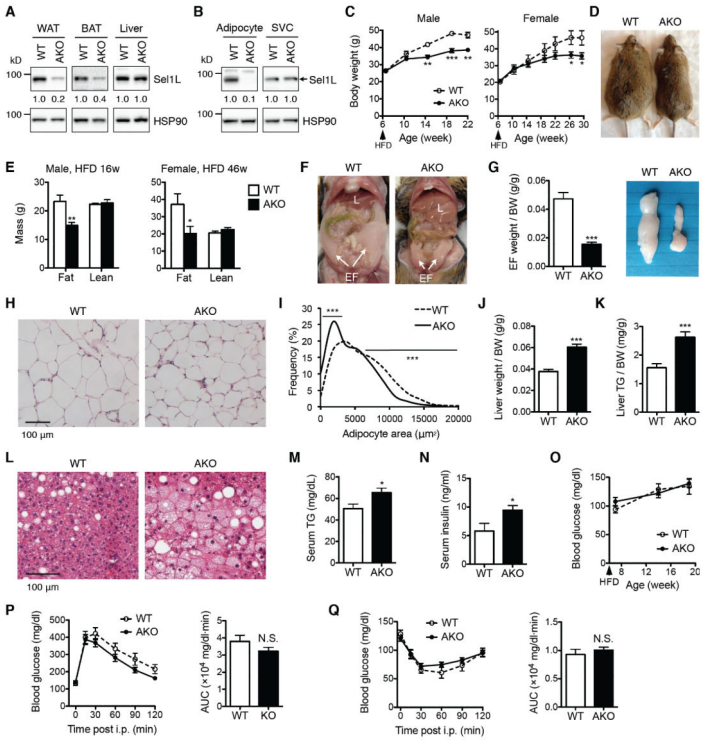

Figure 1. Resistance to Diet-Induced Obesity and Altered Lipid Distribution in AKO Mice

(A-B) Immunoblots of Sel1L in white/brown adipose tissues (WAT/BAT) and liver of WT and AKO mice (A), and in primary adipocytes and stromal vascular cells (SVC) isolated from WAT

(B). Relative Sel1L expression levels normalized to HSP90 shown below the blots.

(C) Body weights of WT and AKO males and females (right) fed HFD (n = 6 each).

(D) Representative picture of WT and AKO female mice fed HFD for 26 weeks.

(E) Fat and lean masses of WT and AKO males (left) and females (right) fed HFD as measured by dual energy X-ray absorptiometry (DEXA) (n = 5-6 each).

(F) Representative pictures of WT and AKO males fed HFD for 16 weeks. L: liver, EF: epididymal fat.

(G) EF weight normalized to body weight (BW) of mice in (F) (n = 11 each). Right, a representative image of EF.

(H) Representative hematoxylin and eosin (H&E) staining of EF sections from mice in (F).

(I) Histogram showing adipocyte area from (H) (n = 990 cells each).

(J-L) Liver weights (J) and total triglyceride (TG) in the liver (K) normalized to BW, and H&E staining of liver sections (L) of WT and AKO mice fed HFD for 16 weeks (n = 10-11 each).

(M) Serum TG levels of 4 h-fasted WT and AKO male mice fed HFD for 16 weeks (n = 6 each).

(N) Serum insulin levels of 4 h-fast male mice fed HFD for 16 weeks as determined by ELISA assay (n = 6 each).

(O) Blood glucose levels in WT and AKO males on HFD after an 18 h fast (n = 6 each).

(P-Q) Glucose and insulin tolerance test (GTT and ITT) on males fed HFD for 13 weeks (n = 6-8 mice each). Right, area under the curve (AUC) analysis.

Data are mean ± SEM. *$p < 0.05$, **$p < 0.01$, ***$p < 0.001$, N.S., not significant by Student's *t* test. HSP90, a loading control. See also Figures S1 and S2.

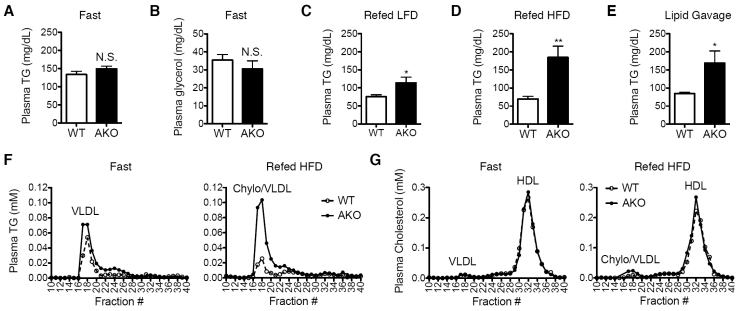

Figure 2. Postprandial Hypertriglyceridemia of AKO Mice

(A-B) Plasma TG (A) and glycerol (B) levels in WT and AKO mice fasted overnight (n = 10-11 each).

(C-D) Plasma TG levels of WT and AKO mice refed LFD for 3 h (C) or HFD for 4 h (D) after an overnight fast (n = 9-12 each).

(E) Plasma TG levels at 2.5 h post-oral gavage with olive oil in mice fasted for 4 h (n=4-6 each).

(F-G) TG (F) and cholesterol (G) levels in lipoproteins by FPLC lipid profile analysis of plasma pooled from WT and AKO mice (n = 5 per genotype) that were either fasted overnight or refed HFD for 4 h following an overnight fast. VLDL, very low-density lipoproteins; Chylo, chylomicrons; HDL, high-density lipoproteins.

Data are mean ± SEM. *$p < 0.05$, **$p < 0.01$, N.S., not significant by Student's *t* test.

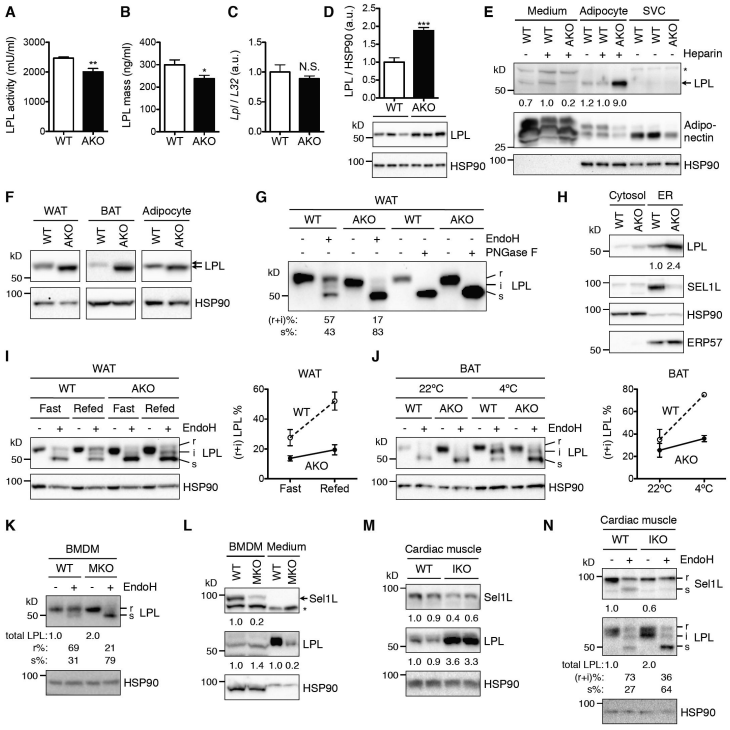

Figure 3. Sel1L Deficiency Leads to ER Retention of LPL

(A-B) LPL activity (A) and LPL mass (B) in post-heparin plasma of LFD mice refed with HFD for 2 h following an overnight fast (n = 4 each).

(C) *Lpl* mRNA levels in WAT of WT and AKO mice fed LFD by qPCR and normalized to *L32* (n = 6 each).

(D) Immunoblots and quantitation (upper) of LPL in WAT of WT and AKO mice fed LFD (n = 4-5 each).

(E) Immunoblots of LPL and adiponectin in the culture medium of primary adipocytes, adipocytes and SVC. Primary adipocytes isolated from WAT of LFD mice were cultured and incubated for 6 h in the presence of 1 μg/ml insulin with or without 10 U/ml heparin. Quantitation of protein levels relative to WT (with heparin) in medium and adipocytes shown below the blot.

(F) Immunoblots of LPL in WAT, BAT and primary adipocytes to show the faster mobility shift of LPL in AKO samples.

(G) Western blot analysis of LPL in WAT lysates treated with endoH or PNGase F. Percent of EndoH resistant (r) + intermediate (i) and sensitive (s) LPL in total LPL shown below.

(H) Representative immunoblots in the ER-enriched and cytosol fractions of WT and AKO WAT from two repeats. Quantitation of LPL shown below the blot.

(I-J) Immunoblots of LPL in endoH-treated WAT lysates of mice fasted overnight with or without refeeding with HFD for 2 h (I) or BAT lysates of mice that were kept at either 22°C or 4°C for 4 h following an overnight fast (J). Right, quantitation of the percent of r+i LPL in total LPL (n = 3-4 each as shown in Figure S3E-F).

(K) Western blot analysis of LPL in endoH-treated BMDM lysates from WT and macrophage-specific *Sel1L* deficient (MKO) mice.

(L) Immunoblots of Sel1L and LPL in cell lysates and culture medium of BMDM from WT and MKO mice after incubation for 3 h in the presence of 10 U/ml heparin. LPL levels relative to WT in BMDM and medium were shown below the blot.
(M-N) Western blot (M) and endoH (N) analysis of LPL in the heart lysates from WT and inducible *Sel1l* knockout (IKO) mice. Quantitation shown below the gel.
Data are mean ± SEM. *$p < 0.05$, **$p < 0.01$, N.S., not significant by Student's *t* test. HSP90, a loading control. *, a non-specific band. a.u., arbitrary unit. See also Figure S3.

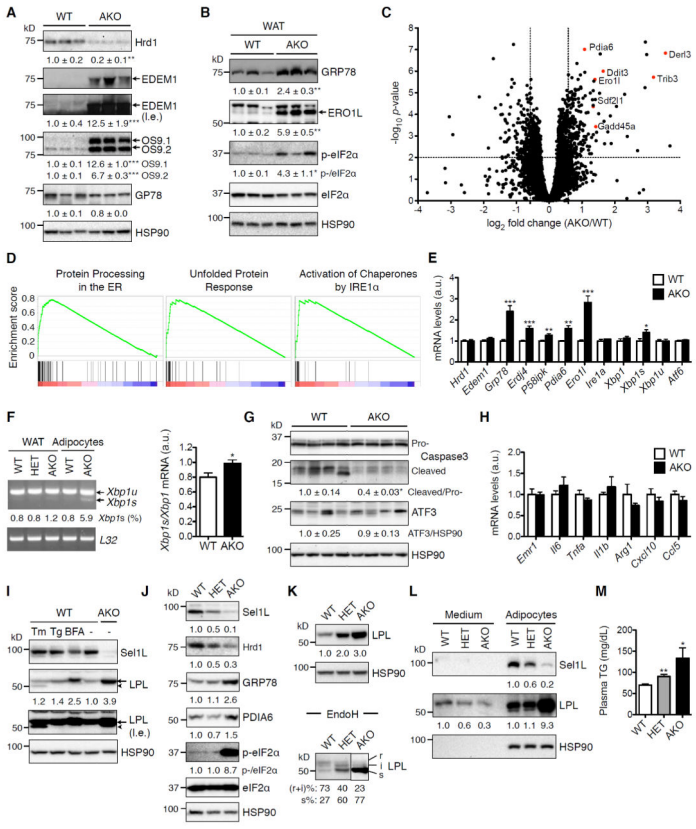

Figure 4. ERAD Defect and UPR Activation in the WAT of AKO Mice and Haploinsufficiency of Sel1L on LPL Secretion

(A-B) Immunoblots of ERAD (A) and UPR (B) genes in WAT of WT and AKO mice fed HFD for 16 weeks. Protein levels normalized to HSP90 shown below the blots (n = 3-6 each).

(C) Volcano plot of Affymetrix microarray analysis of WAT from WT and AKO mice fed HFD for 5 weeks (n = 4 each) with top upregulated UPR/ERAD genes highlighted.

(D) Top three upregulated pathways in AKO WAT by gene set enrichment analysis (GSEA) of Affymetrix microarray in (C) (false discovery rate or FDR q < 0.0002).

(E) qPCR analysis of UPR genes normalized to *L32* in WAT of mice fed HFD for 16 weeks (n = 6 each).

(F) RT-PCR and qPCR analyses of *Xbp* mRNA splicing in WAT and primary adipocytes. HET, adipocyte-specific *Sel1l*$^{+/-}$ mice. *L32*, a loading control. Percent of *Xbp1s* in total *Xbp1* (*Xbp1u* + *Xbp1s*) shown below. Right, relative ratio of *Xbp1s* to total *Xbp1* mRNA levels in WAT of WT and AKO mice by qPCR (n = 6 each).

(G) Immunoblots of Caspase3 and ATF3 in WAT of WT and AKO mice fed HFD for 16 weeks. The ratio of cleaved to pro-Caspase3 and protein level of ATF3 shown below the blots (n = 6 each).

(H) Inflammatory gene expression normalized to *L32* in WAT of mice fed HFD for 16 weeks by qPCR (n = 6 each).

(I) Immunoblots of LPL in primary adipocytes either mock-treated (-) or treated with 5 μg/ml tunicamycin (Tm), 300 nM thapsigargin (Tg) or 1 μg/ml brefeldin A (BFA) in the presence of 1 μg/ml insulin for 4 h. Arrowhead points to the deglycosylated LPL in Tm-treated samples.

(J-K) Immunoblots of UPR genes (J) and LPL (K) in WAT of WT, HET and AKO mice refed LFD for 4 h after an overnight fast. In K, endoH analysis of LPL shown below.

(L) Immunoblots of Sel1L and LPL in the culture medium and cells of primary adipocytes from WT, HET and AKO mice incubated for 4 h with 2 μg/ml insulin and 10 U/ml heparin. Protein levels relative to WT shown below the blot.

(M) Plasma TG levels of WT, HET and AKO mice refed HFD for 4 h after an overnight fast (n = 6 each).

Data are mean ± SEM. *$p < 0.05$, **$p < 0.01$, ***$p < 0.001$ by Student's *t* test. HSP90, a loading control. l.e., long exposure. a.u., arbitrary unit. See also Figures S4-S6.

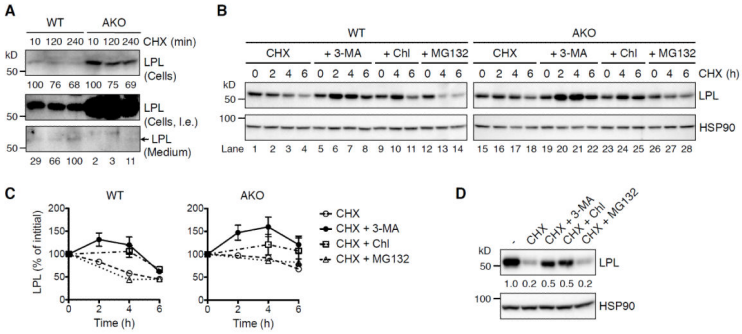

Figure 5. LPL Degradation Is Mediated by Autophagy, Independently of ERAD and Proteasome

(A) Western blot analysis of LPL in culture medium and cells of primary adipocytes treated with 50 μg/ml cycloheximide (CHX) for the indicated time. LPL protein levels were normalized to that at 10 min, and LPL levels in the medium relative to WT at 240 min shown below the blots. l.e., long exposure.

(B) Western blot analysis of LPL in primary adipocytes maintained in 1 μg/ml BFA and 1 μg/ml insulin, and treated with 50 μg/ml CHX in the presence or absence of 5 mM 3-methyladenine (3-MA), 200 μM chloroquine (Chl), or 25 μM MG132 for the indicated time.

(C) Quantitation of LPL as in (B) from three experiments.

(D) Immunoblots of LPL in 3T3-L1 adipocytes mock-treated or treated with 50 μg/ml CHX with or without MG132, Chl, and 3-MA for 6 h. Cells were cultured in the presence of 0.4 μg/ml BFA and 1 μg/ml insulin.

Data are mean ± SEM. HSP90, a loading control. See also Figure S6.

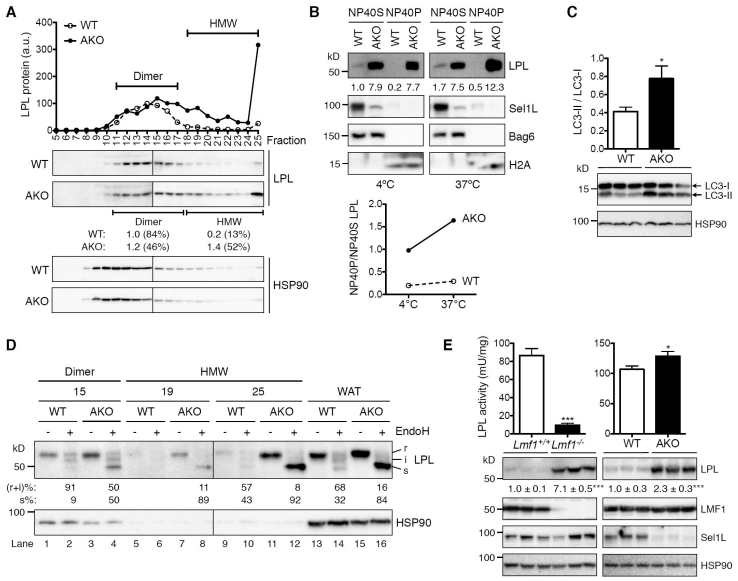

Figure 6. Sel1L Regulates the ER exit of LPL Dimers and Prevents LPL Aggregation

(A) Sucrose gradient analysis of LPL in WAT lysates from WT and AKO mice refed HFD for 3 h following an overnight fast. Quantitation of LPL mass in each fraction shown above. Fractions with LPL dimers and high molecular weight (HMW) complex are indicated. Relative amount and percent of LPL in each configuration shown below the blot.

(B) Immunoblots of LPL in the NP40-soluble (NP40S) and –insoluble (NP40P) fractions of primary adipocytes cultured at 4°C or 37°C for 3 h. Bag6 and H2A mark the NP40S and PN40P fractions, respectively. Quantitation of LPL shown below the blots. A line graph is shown below to illustrate the dynamic movement of LPL from NP40S to NP40P at 37°C.

(C) Quantitation and immunoblots (lower) of LC3 in WAT of WT and AKO mice refed HFD for 3 h following an overnight fast (n=6 each).

(D) EndoH analysis of LPL in the fractions and WAT lysates collected from panel (A). Quantitation of the percent of each LPL form shown below the blots.

(E) LPL activity and immunoblots of LPL, Sel1L and LMF1 (below) in WAT of *Lmf1*$^{+/+}$ and inducible *Lmf1*$^{-/-}$ mice (left, n = 3 each) and WAT of WT and AKO mice refed HFD for 3 h following an overnight fast (right, n = 6 each). Quantitation of LPL mass shown below the blot.

Data are mean ± SEM. *$p < 0.05$, ***$p < 0.001$ by Student's *t* test. HSP90, a loading control.

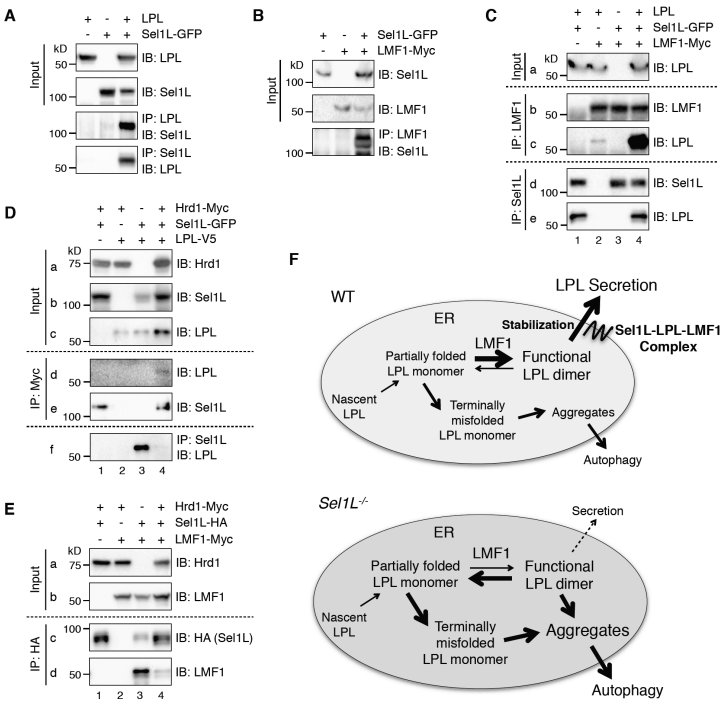

Figure 7. Sel1L Forms a Complex with LPL and LMF1, Independently of Hrd1

(A) Sel1L interacts with LPL. Co-immunoprecipitation (Co-IP) analysis in LPL and Sel1L-GFP-transfected HEK293T cells.

(B) Sel1L interacts with LMF1. Co-IP analysis in Sel1L-GFP and LMF1-Myc-transfected HEK 293T cells.

(C) Sel1L enhances the interaction between LPL and LMF1. Co-IP analysis in LPL, Sel1L-GFP and LMF1-Myc-transfected HEK 293T cells.

(D) Hrd1 competes with LPL for Sel1L. Co-IP analysis in Hrd1-Myc, Sel1L-GFP and LPL-V5-transfected HEK 293T cells.

(E) Hrd1 competes with LMF1 for Sel1L. Co-IP analysis in Hrd1-Myc, Sel1L-HA and LMF1-Myc transfected HEK 293T cells.

(F) A model for Sel1L-regulated LPL secretion. LMF1 is responsible for the maturation of LPL monomers into functional dimers. Sel1L may stabilize LPL dimers through the Sel1L-LPL-LMF1 complex, allowing the ER exit of LPL dimers. In Sel1L-deficient cells (lower), LPL dimers become unstable, trapped in the ER, dissociate into monomers and form aggregates. LPL aggregates are degraded primarily by autophagy.

See also Figure S7.